# Letters

# A PCB-Integrated Inductor With an Additively Electrodeposited Laminated NiFe Core for MHz DC–DC Power Conversion

Yixiao Ding, Xuan Wang, and Mark G. Allen, *Fellow, IEEE*

***Abstract*—A printed circuit board (PCB) integrated inductor with an additively electrodeposited polypyrrole-laminated nickel-iron (NiFe) core is presented for MHz dc–dc power conversion. The PCB-integrated inductor has a racetrack-shaped winding, which is formed using a standard PCB manufacturing process. Subsequently, multilayers of NiFe and polypyrrole are electrodeposited to wrap a laminated core around the PCB racetrack winding. A 515 nH PCB-integrated inductor is fabricated. The fabricated inductor shows a dc resistance of 290 mΩ and a peak quality factor of 9.6 at 2.1 MHz. The inductor is tested in a 4 MHz buck converter and achieves an inductor efficiency higher than 85.0% over a wide range of output currents (0.15–0.4 A).**

***Index Terms*—Dc–dc converter, electrodeposition, integrated inductor, laminated magnetic core, printed circuit board (PCB), power system in package.**

## I. Introduction

MINIATURIZATION of dc–dc converters is driven by the advancement of modern electronic devices, such as consumer electronic devices and IoT devices. These devices exhibit a growing demand for compactness, functionality, and energy efficiency. Such demand can be addressed by placing miniaturized voltage converters close to their loads (different functional blocks), which reduces dc–dc distribution losses, the stray inductance, and improves transient response.

A major bottleneck of miniaturizing dc–dc converters is downsizing the bulky discrete passive components, namely capacitors and inductors. Increasing the switching frequency of converters into the MHz range allows for reduced values of passive components [1]. To further reduce the size of inductors, magnetic core materials with high permeability and saturation flux density can be employed. Additional converter compactness can be achieved by fabricating passive elements directly into the package itself [2], [3], [4], [5], [6], [7], [8], [9], [10], [11], [12]. In this approach, converter IC chips and other components can be soldered on or wire bonded to passive-bearing substrates, achieving a compact power system in package (PwrSiP).

There have been numerous efforts over many years to develop small-scale magnetic-core inductors for compact converters [2], [3], [4], [5], [6], [7], [8], [9], [10], [11], [12], [13], [14], [15], [16]. Metallic, composite, or ferrite composite materials are commonly used as inductor magnetic cores; in the case of metallic cores, lamination may be required to suppress eddy currents for higher frequency operation. When fabricating PwrSiP systems, these core materials are typically embedded in the package substrates, such as FR-4 boards, and the inductor windings and package traces are formed subsequently [5], [6], [7], [8], [9], [10]. Pre-embedding of core materials may add complexity to standard printed circuit board (PCB) fabrication processes. Alternatively, additive core realization approaches, including physical vapor deposition and electrodeposition, can be employed for magnetic cores post-PCB fabrication [4], [11], [12]. Compared to physical vapor deposition processes such as sputtering, the use of electrodeposition to realize the magnetic cores can potentially lower the fabrication cost. Physical vapor deposition requires a vacuum-based deposition environment while electrodeposition takes place in ambient environment; furthermore, physical vapor deposition typically has a lower deposition rate. For example, in [14], physical vapor deposition of a 35-$\mu$m-thick magnetic film takes $\sim$29 h, corresponding to a deposition rate of 0.34 nm/s. In contrast, the electrodeposition process has a deposition rate of 2.1 nm/s for nickel-iron (NiFe) material [17], more than six times faster than physical vapor deposition. However, traditional electrodeposition processes typically result in metallic cores and are less compatible with the laminations required for these cores. Therefore, most electrodeposited magnetic cores typically have a limited thickness to avoid substantial eddy current losses when operating at high frequencies; this limited thickness may ultimately limit the inductance and power handling of these devices. Recently, a fully additive sequential electrodeposition approach for fabricating metal/polymer laminated structures was developed [17], which brings the possibility of electrodeposition of laminated magnetic structures. With the lamination, the total magnetic film thickness can be increased by multiple times, which leads to a larger inductance improvement and better power handling capability [4].

Manuscript received 8 July 2023; revised 12 August 2023; accepted 7 September 2023. Date of publication 22 September 2023; date of current version 23 October 2023. This work was supported by the National Science Foundation National Nanotechnology Coordinated Infrastructure Program under Grant NNCI-2025608, which is carried out at the Singh Center for Nanotechnology. *(Corresponding author: Yixiao Ding.)*

The authors are with the Department of Electrical and Systems Engineering, University of Pennsylvania, Philadelphia, PA 19104 USA (e-mail: yxding@seas.upenn.edu; wxuan@seas.upenn.edu; mallen@upenn.edu).

Color versions of one or more figures in this article are available at https://doi.org/10.1109/TPEL.2023.3318402.

Digital Object Identifier 10.1109/TPEL.2023.3318402

0885-8993 © 2023 IEEE. Personal use is permitted, but republication/redistribution requires IEEE permission.
See https://www.ieee.org/publications/rights/index.html for more information.

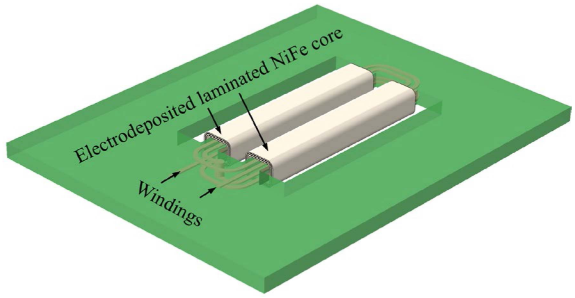


Fig. 1. Schematic 3-D view of the PCB-integrated inductor with an additively electrodeposited polypyrrole-laminated NiFe core.

By combing this electrodeposition technology with a standard PCB manufacturing process, a PCB-integrated inductor with electrodeposited polypyrrole-laminated NiFe cores is developed for MHz dc–dc power conversion.

## II. Inductor Overview

### A. Inductor Architecture

The proposed PCB-integrated inductor with polypyrrole-laminated NiFe core is illustrated in Fig. 1. The racetrack-shaped winding is formed using a low-cost standard two-layer PCB manufacturing process. The winding trace on the top layer and the winding trace on the bottom layer of the PCB are connected in series using plated through holes to increase the inductance. Alternatively, if low resistance is desired, the winding traces on top and bottom layers can be connected in parallel. Three slots surrounding the winding are drilled using the standard PCB manufacturing process. These slots are used to house the inductor core. The core is comprised of multiple alternating NiFe and polypyrrole layers. Both the NiFe and polypyrrole layers are fabricated using the developed sequential electrodeposition process [17]. The conductivity of polypyrrole is more than six orders of magnitude smaller than that of NiFe, enabling the polypyrrole layers to be used as interlamination insulation layers, which can effectively suppress the eddy currents that would otherwise flow between the NiFe layers [18], [19].

A four-turn PCB-integrated inductor is designed for demonstration purposes. There are two-turn windings on each of the top and bottom PCB copper layers, which are connected in series. Considering the constraints of the PCB manufacturing process utilized, the top and bottom windings have a Cu track width/spacing/thickness of 100 $\mu$m/100 $\mu$m/35 $\mu$m. The distance between top and bottom windings is equal to the thickness of the PCB, which is 0.3 mm. While thinner boards are available, which can shorten the magnetic path of the core and increase the inductance, these thicker boards were chosen for convenient handling in the laboratory environment during the core electrodeposition process. The width of the drilled slots is set to be 0.6 mm, the minimum value available in this PCB process. The length of the slots is 5.0 mm for accommodating a 4.6 mm long core. The inductor device has an overall length of 6.0 mm and a width of 1.7 mm, resulting in an area of 10.2 mm$^2$.

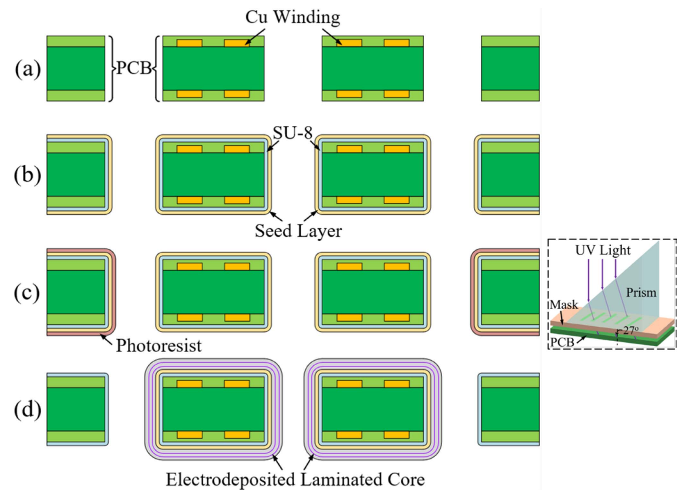


Fig. 2. Major fabrication steps of the PCB-integrated inductor. (a) PCB received from the manufacturer. (b) Spray coating SU-8 and seed layer deposition. (c) Electrodeposition mold formation by photolithography. (d) Electrodeposition of the laminated core.

### B. Fabrication Process

The major fabrication steps are shown in Fig. 2. First, a PCB with copper windings and slots is fabricated at a PCB manufacturing house, as described previously. Fig. 2(a) shows the PCB received from the PCB manufacturer. The received board is cleaned in an ultrasonic bath using acetone and isopropyl alcohol. Subsequently, a layer of SU-8 is spray-coated onto the front and back sides of the board. The SU-8 layer can help planarize the board surface and round the edges of the slots. After curing the coated SU-8 layer, a seed layer of Ti/Cu is sputtered onto the front and back sides of the board [see Fig. 2(b)]. Then, a photoresist layer is spray coated on both sides of the board. The photoresist on the front and back side is patterned to serve as the mold for electrodeposition of the laminated NiFe core [see Fig. 2(c)]. To expose the photoresist on the sidewall of the slots, a right-angle glass prism is positioned on the mask during the exposure, which alters the UV light path [20]. As a result, the UV light becomes inclined after passing through the prism, which ensures complete exposure of the unwanted photoresist on the sidewall to the UV light. Therefore, the unwanted photoresist is removed during the subsequent development step. Next, alternating electrodeposition of NiFe and polypyrrole films within the mold is carried out. A three-bath electrodeposition system is used. In a typical deposition cycle, the NiFe layer is first electrodeposited in a NiFe deposition bath. Then, the polypyrrole layer is electrodeposited onto the previously deposited NiFe layer in a polypyrrole bath. After that, a very thin Ni strike layer is electrodeposited to active the polymer surface for the subsequent NiFe deposition. The deposition cycle of NiFe/Polypyrrole is repeated as needed. The ultimate thickness of the polypyrrole-laminated NiFe structure is limited by the thickness of the electrodeposition mold. More details regarding the electrodeposition step, including bath compositions and plating current densities, can be found in [17]. Finally, after the electrodeposition of the laminated NiFe core, the photoresist mold is removed using acetone. The Ti/Cu seed

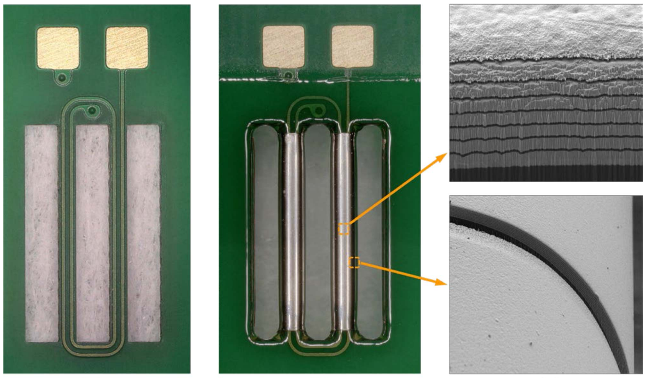

(a) (b) (c)

Fig. 3. (a) PCB with the inductor winding and drilled slots received from the manufacturer. (b) Fabricated PCB-integrated inductor with the electrodeposited polypyrrole-laminated NiFe core. (c) FIB-SEM images of the laminated NiFe core taken at the central position (top) and the edge (bottom) of the core.

layer is removed using a commercial copper etchant (Copper Etch BTP, Transene), followed by a hydrofluoric acid etch [see Fig. 2(d)].

Fig. 3(a) shows the top view of the inductor winding and the drilled slots on the PCB received from the PCB manufacturer, corresponding to Fig. 2(a). Fig. 3(b) shows the top view of the fabricated inductor with the polypyrrole-laminated NiFe core, corresponding to Fig. 2(d). The FIB-SEM images of Fig. 3(c) show the cross-sectional view of the electrodeposited polypyrrole-laminated NiFe core and are taken at different positions of the core. The core comprises 8 layers of NiFe (the gray layers) and 7 layers of polypyrrole (the black layers). The Ni strike layer is too thin to be observed in the FIB-SEM images. The thickness of each NiFe layer and polypyrrole layer was measured to be ∼1.5 um and ∼300 nm, respectively. The total thickness of the laminated core is ∼14 um. As shown in the bottom FIB-SEM image of Fig. 3(c), the lamination feature is well maintained at the edge transition region from the flat top surface to the sidewall.

## III. Results and Discussion

The dc resistance of the fabricated PCB-integrated inductor is measured to be 290 mΩ using the four-point probe method with a Keithley 2450 source meter. The ac characterization is performed with an Agilent E5061B Network Analyzer and a GGB ECP18-SG-1250-DP RF probe. Prior to the ac characterization, a standard short-open-load calibration is made. The results of the ac measurement are shown in Fig. 4. The inductor has a nearly constant inductance of 515 nH up to 10 MHz. The quality factor is higher than 5 from 400 KHz to 7 MHz and reaches a peak value of ∼9.6 at 2.1 MHz. It is noted that the ac resistance begins to drop at ∼26 MHz. The reason for this drop is due to the eddy current effect at higher frequencies. The eddy currents will prevent the high-frequency magnetic field from penetrating the NiFe layers, which results in the decreased inductance and also reduces the total power loss naturally. If inductors need to be operated at a higher frequency range, the thickness of NiFe and polypyrrole layers can be adjusted correspondingly to effectively suppress the eddy current effect.

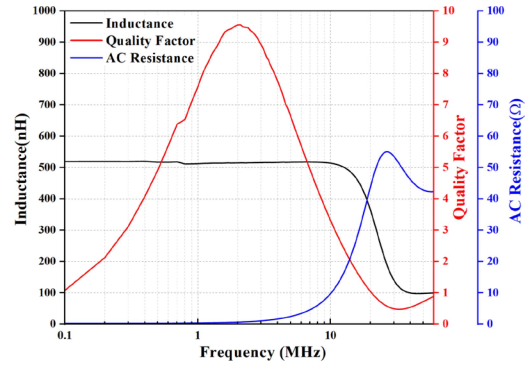


Fig. 4. Measured ac performance of the fabricated inductor.

Due to the relatively large dimension of the inductor compared to the thickness of the NiFe layers, the magnetic path length of each NiFe layer is nearly the same, which leads to a uniform distribution of magnetic flux in the core. Based on the magnetic path length of the fabricated inductor and the magnetic property of the laminated NiFe material, the saturation current is estimated to be ∼500 mA. In our demonstration, the magnetic material is isotropic, and the magnetic core has no air gaps. To further improve the saturation current, the hard axis of the magnetic core can be aligned with the flux direction, and air gaps can be introduced by changing the photomask pattern.

Compared with silicon-based thin film inductors [14], [15], [16], the fabricated inductor shows an $L/R_{DC}$ ratio of 1776 nH/Ω while the silicon-based thin film inductors exhibit an $L/R_{dc}$ ratio ranging from 434 to 1416 nH/Ω. This is attributable to the thick inductor winding enabled by standard PCB processes, which is typically unavailable on silicon substrates. Regarding inductance density, the fabricated inductor has an inductance density of 50 $nH/mm^2$. Although the inductor has a relatively large size and, thus, a long magnetic path length, the electrodeposited core is thicker than that of the silicon-based inductors. Therefore, the inductance density is comparable to that of the silicon-based thin film inductor, which ranges from 24 to 133 $nH/mm^2$. Compared with the other PCB-integrated inductors [5], [6], [7], [8], [9], [10], in which the cores are typically made of ferrite, ferrite composite, or metallic composite, the electrodeposited core of the fabricated inductor has a higher permeability. Therefore, the inductance density of the fabricated inductor is higher than that of previous PCB-integrated inductors, which range from 5 to 31 $nH/mm^2$ [5], [6], [7], [8], [9], [10]. The $L/R_{dc}$ ratio of other PCB-integrated inductors with embedded cores is 208–14015 nH/Ω. For the proposed inductor, it is also possible to achieve a higher $L/R_{dc}$ ratio using multiple PCB copper layers as windings.

The fabricated inductor is tested on a dc–dc converter evaluation board (TPS628510EVM, Texas Instruments) by replacing a commercial inductor on the board with the fabricated inductor, as shown in Fig. 5(a). Details of the converter chip and the evaluation board can be found in [21] and [22]. During the board-level test, the converter operates in pulsewidth modulation mode with a fixed switching frequency of 4 MHz. The input and output voltages of the converter are 2.7 V and 1.8 V, respectively.

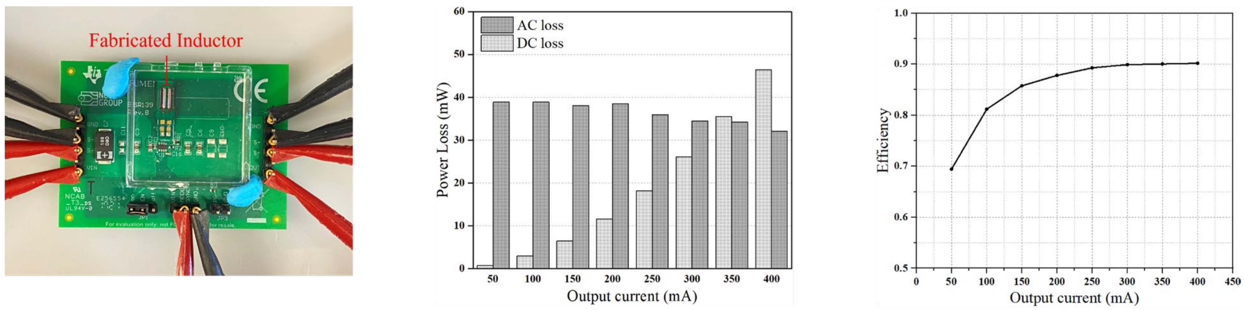


(a) (b) (c)

Fig. 5. Fabricated inductor tested in a 4 MHz, 2.7 V – 1.8 V dc–dc converter. (a) Inductor tested on the dc–dc converter board. (b) Inductor loss breakdown across output current. (c) Inductor efficiency across output current.

The output current ranges from 50 mA to 400 mA. To separate the inductor power loss from the measured total power loss, a previously reported power loss breakdown method is used [16]. An air-core PCB inductor is also tested on the evaluation board under the same test conditions. The inductance of the air-core inductor is similar to that of the fabricated inductor. The dc and ac performance of the air-core inductor are determined by small-signal characterization. Using the known ac resistance, dc resistance and inductance of the air-core inductor, the power loss of the air-core inductor is calculated. Therefore, the total power loss of the converter using the air-core inductor can be separated into two major losses: the air-core inductor loss and all other losses associated with the converter board. Since the test conditions and the converter board used are identical for both inductors, the board loss observed in the converter with the air-core inductor is used to estimate the power loss of the fabricated inductor. The total power loss of the fabricated inductor is further separated into dc loss, calculated based on the measured dc resistance, and ac loss, which is obtained by subtracting the dc loss from the total inductor power loss. The loss breakdown of the fabricated inductor is shown in Fig. 5(b). The dc loss increases with the increase of the output current. The ac loss remains nearly constant across the measured output current range because of the constant current ripple through the inductor. At the low output current range, the ac loss dominates compared to the dc loss. The ac loss, including the ac winding loss and magnetic core losses, is dominated by the latter. When the output current reaches $\sim$300 mA, the magnetic core loss is approximately equal to the total dc and ac winding loss. The core losses consist of eddy current core loss and hysteresis core loss. Since the core is laminated, the eddy current core loss has been suppressed. For the fabricated inductor, the core is isotropic. By aligning the hard axis of the core to the magnetic field direction, which can help reduce the hysteresis loss, the magnetic core loss can be further reduced. This can be realized by applying an external magnetic field during the core electrodeposition [13].

The efficiency of the fabricated inductor at different output currents is shown in Fig. 5(c), which is commonly defined by the following equation [15]:

$$\eta_{\text{IND}} = \frac{V_O I_O}{V_O I_O + P_{\text{LOSS,IND}}} \tag{1}$$

where $P_{\text{LOSS, IND}}$ are the inductor loss, and $V_O$ and $I_O$ are the output voltage and output current of the converter, respectively. An inductor efficiency higher than 85.0% is maintained over a wide range of output currents (0.15–0.4 A). A maximum inductor efficiency of 90.2% is achieved at a 0.4 A output current. The efficiency is comparable to that of the air-core PCB inductor, which has an efficiency of 92.6% at a 0.15 A output current and drops to 86.2% at a 0.4 A output current. However, the integrated inductor occupies only $\sim$58% of the area of the air-core inductor.

In this demonstration, the inductor has a relatively large area of 10.2 mm$^2$. A significant portion of the area is unused due to the limitations imposed by the adopted PCB process, particularly in terms of slot size. If an advanced process is employed, such as using a laser to drill the slots, the slot width can be reduced to 0.1 mm, which is wide enough to house the inductor core. As a result, the total area can be reduced to 7.2 mm$^2$. Further reduction in area can be achieved by utilizing a smaller winding spacing and smaller plated-through holes.

The proposed inductor is fabricated on a PCB, which is manufactured using a standard PCB manufacturing process, and wiring and pads for other converter components can also be formed using the same PCB process. Following the inductor formation, the PCB can still serve as a substrate, and other components can be integrated on the PCB to achieve an integrated power converter solution. Due to the electrodeposited core wrapping around the PCB, other components may need to be placed side by side with the inductor. However, the possibility of placing some large components on top of the inductor that span the inductor width, such as connectors or capacitors, can also be envisaged.

To meet different requirements of power converters, the inductance of the proposed PCB-integrated inductor can be adjusted by changing the core and winding design. First, the thickness of the magnetic core can be adjusted through controlling the electrodeposition condition. Second, the core shape can be adjusted, such as using a different core length or introducing airgaps. This can be realized by modifying the photomask design. Also, the inductance can be adjusted by the winding design, such as the number of turns.

The developed process provides a general approach to fabricate a structure, which has conductive windings wrapped by the laminated NiFe material. Different inductor shapes, such as pot-core inductors, strip-line inductors, meander inductors, and toroidal inductors, can also be realized using the developed process or by adding additional steps. Alternatively, it is possible to consider embedding the multilayer electrodeposited NiFe material into the PCB and fabricate integrated inductors in an embedded fashion.

## IV. Conclusion

A PCB-integrated inductor with electrodeposited polypyrrole -laminated NiFe cores has been experimentally demonstrated. The developed fabrication process takes advantage of the low-cost standard PCB manufacturing process and fully additive electrodeposition of laminated cores. The fabricated inductor has a high L/$R_{dc}$ ratio of 1776 nH/$\Omega$ and a peak quality factor of 9.6 at 2.1 MHz. The on-board test of the inductor shows a good inductor efficiency for a 4 MHz buck converter application. This new PCB-integrated inductor is promising for power system-in-package applications.

## Acknowledgment

The authors would like to thank Prof. J. K.O. Sin at the Hong Kong University of Science and Technology for his excellent support in the characterization of the inductors and like to thank Dr. J. B. Pyo for his valuable suggestions on the electrodeposition process.

## References

[1] C. O. Mathúna, N. Wang, S. Kulkarni, and S. Roy, “Review of integrated magnetics for power supply on chip (PwrSoC),” *IEEE Trans. Power Electron.*, vol. 27, no. 11, pp. 4799–4816, Nov. 2012.

[2] J. Y. Park and M. G. Allen, “Low temperature fabrication and characterization of integrated packaging-compatible ferrite-core magnetic devices,” in *Proc. IEEE Appl. Power Electron. Conf. Expo.*, 1997, pp. 361–367.

[3] S. C. Tang, S. Y. R. Hui, and H. S. H. Chung, “A low-profile power converter using printed-circuit board (PCB) power transformer with ferrite polymer composite,” *IEEE Trans. Power Electron.*, vol. 16, no. 4, pp. 493–498, Jul. 2001.

[4] M. Ludwig, M. Duffy, T. O’Donnell, P. McCloskey, and S. C. O. Mathuna, “PCB integrated inductors for low power DC/DC converter,” *IEEE Trans. Power Electron.*, vol. 18, no. 4, pp. 937–945, Jul. 2003.

[5] T. Sun et al., “Substrate-embedded low-resistance solenoid inductors for integrated voltage regulators,” *IEEE Trans. Compon. Packag. Manuf. Technol.*, vol. 10, no. 1, pp. 134–141, Jan. 2020.

[6] R. Murphy et al., “PCB embedded toroidal inductor for 2MHz point-of-load converter,” in *Proc. IEEE 11th Int. Conf. Integr. Power Electron. Syst.*, 2020, pp. 1–5.

[7] C. Alvarez et al., “Demonstration of a high-inductance high-density and low DC resistance compact embedded toroidal inductor for IVR,” in *Proc. IEEE 71st Electron. Compon. Technol. Conf.*, 2021, pp. 1293–1299.

[8] K. Bharath et al., “Integrated voltage regulator efficiency improvement using coaxial magnetic composite core inductors,” in *Proc. IEEE 71st Electron. Compon. Technol. Conf.*, 2021, pp. 1286–1292.

[9] W. Zhang et al., “Embedded magnetic solenoid inductor into organic packaging substrate using lithographic via technology for power supply module integration,” *IEEE Trans. Electron Devices*, vol. 69, no. 9, pp. 5116–5122, Sep. 2022.

[10] F. Zhu and Q. Li, “A novel PCB-embedded coupled inductor structure for a 20MHz integrated voltage regulator,” *IEEE J. Emerg. Sel. Topics Power Electron.*, vol. 10, no. 6, pp. 7452–7463, Dec. 2022.

[11] J. Qiu and C. R. Sullivan, “Design and fabrication of VHF tapped power inductors using nanogranular magnetic films,” *IEEE Trans. Power Electron.*, vol. 27, no. 12, pp. 4965–4975, Dec. 2012.

[12] Y. Wu and H. Yu, “A low-cost novel method to fabricate integrated magnetic core inductor embedded in organic substrate,” *IEEE Trans. Magn.*, vol. 58, no. 8, Aug. 2022, Art. no. 8401605.

[13] J. Kim, M. Kim, J.-K. Kim, F. Herrault, and M. G. Allen, “Anisotropic nanolaminated CoNiFe cores integrated into microinductors for high-frequency DC-DC power conversion,” *J. Phys. D Appl. Phys.*, vol. 48, no. 46, Oct. 2015, Art. no. 462001.

[14] D. V. Harburg et al., “Microfabricated racetrack inductors with thin-film magnetic cores for on-chip power conversion,” *IEEE J. Emerg. Sel. Topics Power Electron.*, vol. 6, no. 3, pp. 1280–1294, Sep. 2018.

[15] L. Peng et al., “Silicon-based ultimate miniature magnetic inductors technology for high-efficiency DC-DC conversion,” in *Proc. IEEE Int. Symp. Power Semicond. Devices ICs*, 2020, pp. 384–387.

[16] S. Peng et al., “A micro-inductor with thin film magnetic core for a 20 MHz buck converter,” *J. Magnetism Magn. Mater.*, vol. 524, Apr. 2021, Art. no. 167661.

[17] M. Synodis, J. B. Pyo, M. Kim, H. Oh, X. Wang, and M. G. Allen, “Fully additive fabrication of electrically anisotropic multilayer materials based on sequential electrodeposition,” *J. Microelectromech. Syst.*, vol. 29, no. 6, pp. 1510–1517, Dec. 2020.

[18] M. Kim and M. G. Allen, “Interlamination insulation design considerations for laminated magnetics operating at high frequencies,” *IEEE Trans. Magn.*, vol. 55, no. 8, Aug. 2019, Art. no. 2801511.

[19] J. B. Pyo, X. Wang, M. Kim, H. Oh, R. Kauffman, and M. G. Allen, “Suppression of eddy current loss in multilayer NiFe-Polypyrrole magnetic cores fabricated using a continuous electrodeposition process,” *IEEE J. Emerg. Sel. Topics Power Electron.*, vol. 10, no. 6, pp. 7433–7440, Dec. 2022.

[20] G. Jiang, S. Baig, and M. R. Wang, “Prism-assisted inclined UV lithography for 3D microstructure fabrication,” *J. Micromechanics Microeng.*, vol. 22, no. 8, 2012, Art. no. 085022.

[21] Texas Instruments, “TPS62851x 2.7-V to 6-V, 0.5-A, 1-A, 2-A, and 3-A step-down converters in a SOT583 package,” SLUSDO4B datasheet, Aug. 2020, [Revised Jun. 2022].

[22] Texas Instruments, “TPS62851xEVM-139 evaluation module,” LVUBY6A datasheet, Aug. 2020, [Revised Jun. 2022].